Journal of Materials Science: Materials in Electronics (2018) 29:18891–18904
https://doi.org/10.1007/s10854-018-0074-1

REVIEW

Carbon nanoscrolls: synthesis and applications

Hongdong Liu[1] · Tao Le[2] · Lei Zhang[2] · Maowen Xu[3]

Received: 30 July 2018 / Accepted: 17 September 2018 / Published online: 18 September 2018

Abstract
Carbon nanoscrolls (CNSs), as an emerging family member of carbon nanomaterials, are a spirally wrapped 2D graphene sheet with a 1D tubular structure resembling that of multi-walled carbon nanotube. Due to its unique topological structure, CNSs not only share the remarkable mechanical, electronic properties and thermal conductivity exhibited by carbon nanotubes and graphene but also are expected to exhibit novel features. So they have attracted much attention from material scientists, chemists and physicists. Here, we review the research advances of preparative strategies of 1D CNSs with arc-discharge, CVD, self-scrolling, freeze-drying, cold quenching, functional groups/nanoparticles modification, mechanical ball milling, ultrasound-assisted and Langmuir–Blodgett methods, and potential applications in lithium ion/sulfur bateries, fuel Cells, supercapacitors, hydrogen storage, sensors, oscillators, photocatalytic materials and the other applications. We believe that CNSs will become another bright star after CNTs and graphene in the foreseeable future.

1 Introduction

Graphite has a three dimensional (3D) laminated structure, where the carbon atoms on the same plane are in SP^2 hybridization. In graphite crystal, the interlayer spacing is 0.34 nm, which is relatively large, and the layer is bonded with another layer via van der Waals force.The individual layer of graphite is called graphene, that is the name given to a flat monolayer of carbon atoms tightly packed into a 2D honeycomb lattice [1–3]. Since its discovery in 2004, it has attracted extensive attentions of worldwide material scientists, chemists and physicists because of its high theoretical specific surface area (2630 $m^2 g^{-1}$) [4], outstanding thermal conductivity (5000 $W m^{-1} K^{-1}$) [5] and mechanical property (1060 GPa) [6], high electron mobility at room temperature (25,000 $cm^2 V^{-1} s^{-1}$) [7], half-integer quantum hall effect and permanent conductivity [8–10]. Therefore, Geim and Novoselov, the discoverers of graphene, win Nobel Prize in physics in 2010. Graphene has bacome another great discovery, following carbon nanotubes (CNTs) and fullerene balls. It can be wrapped up into 0D fullerenes, rolled into 1D nanotubes or stacked into 3D graphite [11], as shown in Fig. 1.

Carbon nanotubes (CNTs) are a typical 1D nano-materials, of which the tubewalls are thought to be formed by rolling single-layer or multi-layer graphene and then seamlessly integrating them. They own a hemisphere cap of graphene on the top and hollow cavity structure inside of the nanotubes. Since CNTs were prepared for the first time in 1991 by Iijima et al. using arc discharge method [12], the preparation methods of CNTs have been developed in diversitification, including chemical vaporous deposition (CVD) [13], laser evaporation method [14], ion beam method [15], solar energy method [16], electrolytic method [17], supercritical fluid method [18], submerged arc method [19], solution combustion method [20] and hydrothermal synthesis method [21], etc. However, the existing CNTs prepared by current methods generally have many defects and are uneasy to be dispersed, which significantly limits the properties and industrial application of CNTs.

Carbon nanoscrolls (CNSs) are another typical 1D nanomaterials, which own an open tubular structure, have attracted considerable attention recently [22–24]. As shown in Fig. 2, these carbon-based materials exhibit a spiral

✉ Lei Zhang
leizhang0215@126.com

✉ Maowen Xu
xumaowen@swu.edu.cn

[1] Chongqing Key Laboratory of Micro/Nano Materials Engineering and Technology, Chongqing University of Arts and Sciences, Chongqing 402160, People's Republic of China

[2] College of Life Science, Chongqing Normal University, Chongqing 401331, People's Republic of China

[3] Faculty of Materials and Energy, Southwest University, Chongqing 400715, People's Republic of China

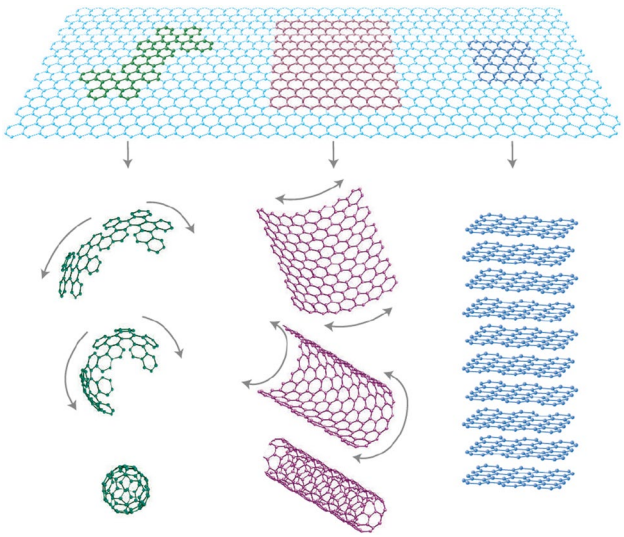

Fig. 1 Mother of all graphitic forms. Graphene is a 2D building material for carbon materials of all other dimensionalities. It can be wrapped up into 0D buckyballs, rolled into 1D nanotubes or stacked into 3D graphite. Reproduced from Ref. [11] .Copyright 2007 nature Publishing Group

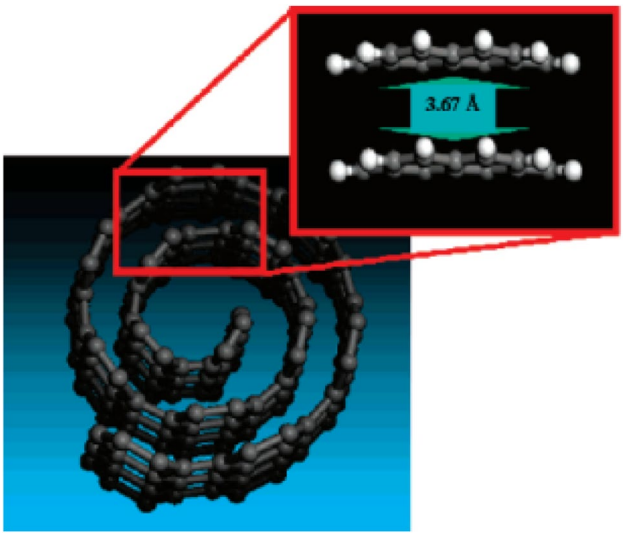

Fig. 2 CNSs and CNSs-model system that consists of two curved graphene layers cut from the corresponding CNSs. Reproduced from Ref. [27]. Copyright 2007 American Chemical Society

architecture and can be schematically rolled up by a twisting of 2D graphene sheet, which is distinct from the seamless concentric structure of multiwalled carbon nanotubes (MWCNTs) [25–27]. Theirs scrolled structure was first proposed by Bacon [28] in 1960 to explain the structure of graphite whiskers grown in electric arch, and later (1993) confirmed by Dravod [29]. CNSs not only inherit excellent mechanical property, electrical and thermal conductivity of 2D graphene, but also provide interlayer galleries that can be intercalated with donors and acceptors, and the nanotube diameter can expand to accommodate the volume of the intercalant. These features are potentially important for a rich variety of applications [30, 31].

2 Mechanism for the formation of CNSs

Molecular dynamics simulations and theoretical analysis have been conducted to investigate mechanisms governing the formation of CNSs from graphene monolayer [32–34]. Simulations reveal that a large enough overlap between two edges of a freestanding graphene monolayer can lead to further relative sliding of the overlapped area and finally forming a CNS [35]. CNSs formation is dominated by two major energetic contributions, the elastic energy (E_{bend}) increase generated by bending the graphene sheet and the free energy decrease caused by the van der Waals interaction energy (E_{VDW}) of overlapping regions of the graphene sheet. Braga et al. discussed CNSs formation by molecular dynamics simulations [30]. Figure 3 presents total energy change during the wrapping of a single graphene sheet to make a CNS. There is an increase in the curvature of the graphene sheet to improve the torsion and inversion contributions to sheet strain energy before graphene sheet overlap occurs (configurations 1–8). Thereby, it makes the rolled structure less stable relative to an undistorted graphene sheet. The structural transition of graphene is ascribed to energy assistance. The surface overlapping regions emerge with the rolling continuation (configuration 9) and the van der Waals contributions improve the structural stability. There is a key value of graphene layer overlap above which the rolling process evolves

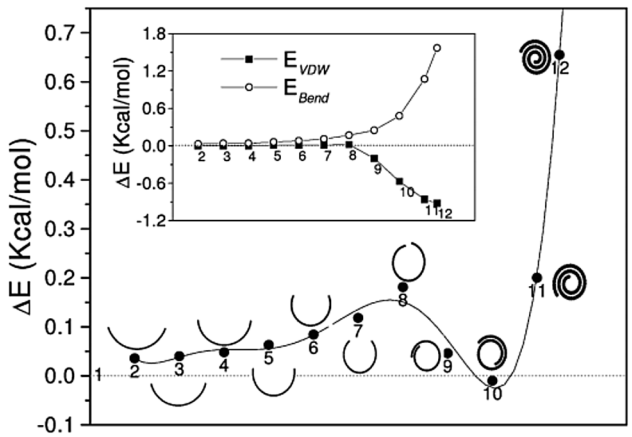

Fig. 3 Change in total energy (relative to an undistorted graphene sheet) during the wrapping of a single graphite sheet to make a CNS. The torsion plus inversion (E_{Bend}) and van der Waals energies (E_{VDW}) are shown in the inset graph. Reproduced from Ref. [30]. Copyright 2004 American Chemical Society

spontaneously due to van der Waals interlayer forces. This critical limit value depends on initial dimensions and orientation of the graphene sheet relative to the axis about which curling takes place. The final structure is more stable than its parent graphene sheet (configuration 10). There is a critical minimum inner diameter (~ 20 Å) for scroll stability according to previous reports [36]. If the bending contributions outweigh the van der Waals energetic gain and the structure becomes unstable for smaller diameters (configurations 11 and 12) [30].

3 Methods of CNSs synthesis

At present, there are lots of methods for preparation CNSs. The general idea is to directly produce CNSs in the preparation process of graphene or CNSs are prepared through two steps: firstly, graphene is formed, and then, CNSs are obtained by certain forces to graphene (such as surface strain, mechanical force, molecules or ions interaction force, etc.). The specific methods are as follows:

3.1 CNSs formed by nucleation-oriented growth

3.1.1 Arc-discharge synthesis

Arc-discharge synthesis is the dominant method for preparing CNTs in early period. This technique process has been significantly improved after many years of development. Early in 1960, Bacon et al. found a hollow curly graphite structure in an arc-discharge experiment of graphite, and defined it as graphite whisker, which was the earliest report on CNSs. The main procedure of this method is to input inert gas into a vacuum pipe, in which a long carbon anode and a short cathode contained a small piece of iron are setted. Then, voltage is applied between the electrodes to realize arc-discharge (Fig. 4) [37]. During the discharge process, the anode is constantly consumed, while the products containing CNSs continuously deposite on cathode [38]. By controlling the catalyst ratio, the diameter of resulting CNSs can be controlled. A possible mechanism of whisker growth is proposed. A thin graphite sheet or ribbon coils itself up in order to reduce its surface energy. The resulting scroll is properly oriented, with its axis parallel to the general growth direction, then it can grow rapidly in the direction of increasing length, while thickening simply by tangential growth in spiral fashion. The tangential growth may stop and be superseded by a new growth layer which nucleates on the whisker surface, the new layer possibly being misoriented with respect to the old by a rotation about the c axis. All of the layers then propagate themselves as the whisker grows in length [28]. Based on the similar growth mechanism, Lavin et al. also prepared a kind of defective CNTs which

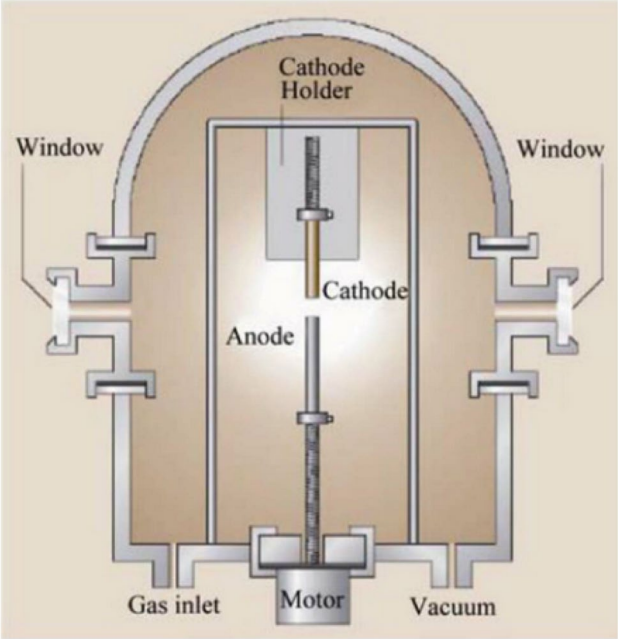

Fig. 4 Arc discharge method. Reproduced from Ref. [37]. Copyright 2011 Scientific Research

is a intermediate product from CNSs to nested MWCNTs through arc-discharge method in helium-atmosphere with open-circuit voltage and current being 20 V and 100 A, respectively. The defect of such MWCNTs varies with theirs thickness [39]. The CNSs prepared by arc-discharge method can be graphitized to the greatest extent and this method is simple and rapid, but there are some disadvantages, for example, the arc discharge is so intense that it is difficult to control the process and the products. The carbon nanoparticles, amorphous carbon or graphite fragments are impurities in the composite, and the impurities are difficult to separate.

3.1.2 CVD

CVD is one of main techniques to prepare CNTs in modern industry. The main process is to decompose carbon-included organic gas (CH_4, C_2H_2, C_2H_4, etc.) at 600–1000 °C in the presence of catalyst, and then conduct low temperature deposition for systhesis of carbon nanomaterials. Kakade et al. prepared large-size CNSs at 680–550 °C in H_2/Ar atmosphere by CVD method using mixture of methylbenzene and ferrocene. The structure and properties of the synthesized products mainly depend on the reaction temperature, and their morphologies can be changed by the reaction temperature [40]. Sebsequently, Schaper et al. decomposed FePc, allowed it to deposite on Si matrix within temperature range of 800–1000 °C, and thus prepared CNSs in the presence of catalyst. The external and internal diameters range of the products are 30–65 nm and 15–40 nm, respectively [41].

Moveover, Chuvilin et al. prepared CNSs with a polygonal cross section using CVD method in H_2/CH_4 atmosphere. The needled-like CNSs have an external diameter of 10–50 nm, while the internal diameter varie of 2–10 nm [42]. Their morphologies are different from that of CNSs produced by catalytic or arc-discharge method. All the CNSs have a non-uniform external diameter as well as a non-uniform diameter of the internal channel. The scroll thickness smoothly decreases toward their ends while the internal channel diameter increases in this direction.

CVD method enjoys some advantages. Such as, easy operation, simple equipment, low-cost raw material, high yield and potential for large-scale production [43, 44]. However, the resulted CNSs often have some crystal defects, uneven diameters and proneness to bending deflection.

3.2 CNSs formed by scrolling induced by surface strain

3.2.1 Self-scrolling of monolayer graphene

In order to reduce the surface energy and achieve the most stable state, the 2D single-layer nanomaterials have the tendency of fold and curl [45]. If graphene is interfered by the external environment, it will be more conducive to curl. Xie et al. took advantage of this phenomenon to immerse the mechanically exfoliated monolayer graphene into a Petri dish filled with isopropyl alcohol (IPA), took it out 5 min later, dried it under nitrogen atmosphere. To their surprise, the graphene turned from a 2D sheet to a 1D fiber-like structure. They explained such phenomenon by four stages in Fig. 5. In the first stage, the chip with graphene was immersed into IPA solution, in which case the upper and lower surfaces of graphene were in contact with IPA and SiO_2. Therefore, a surface strain emerged, which was the driving force for rolling of graphene sheet. In the second stage, under the effect of the surface strain, the graphene edge lifted up from matrix, IPA molecules entered into the space between graphene and matrix, which naturally facilitated the detachment of graphene. In the third stage, due to the perturbation in solution, the detached parts of the graphene curved. In the fourth stage, with the decrease of free energy, the graphene separated from the matrix, and rolled into a CNS bit by bit [46].

Moreover, Li et al. sandwiched the single-layer graphene in polymer matrix with only a few hundred nanometers in thickness, heated it to 150 °C above the polymer's glass temperature, found that the graphene started to curl along the membrane surface. Below the copolymer's glass temperature of about 50 °C, the intertwining of copolymer chains in the matrix acts as a physical restraint and suppresses long distance polymer chain motion. Above glass temperature, the activation energy for cooperative movement

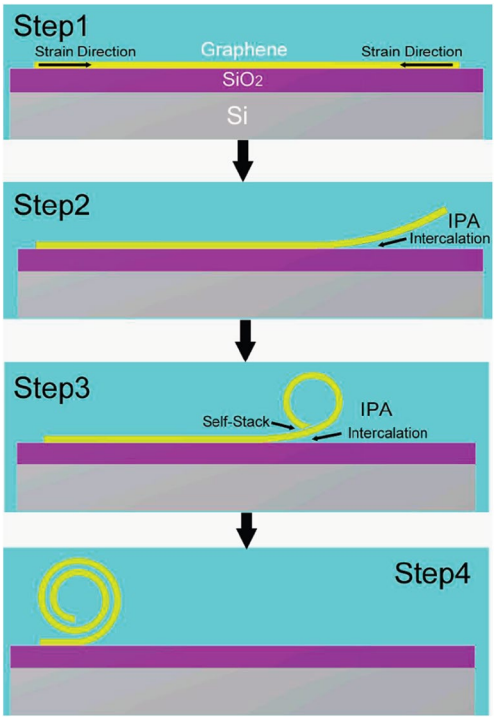

Fig. 5 Schematic representation of the formation of CNS. Step1: surface strain is induced in graphene after it is immersed in IPA solution. Step2: the edge of graphene is lifted up with the help of the surface strain and the intercalation of IPA solution. Step3: the initial bending of the graphene is energetically unfavorable and might be caused by perturbations. Once the graphene gets selfstacked, the scrolling process will be easier. Step4: the graphene continued to roll up until a CNS is formed. Reproduced from Ref. [46]. Copyright 2009 American Chemical Society

of the chain segments is exceeded, which allows the chains to slide past each other when a force is applied, and this increased mobility of the copolymer chains assists their rearrangement during the dislocation of van der Waals force-bonded graphene from the polymer matrix and decreases the free energy cost during the phase transition [47]. After them, Zhou et al. performed spin-coating of polymethyl methacrylate (PMMA) on substrate with lots of graphene, heated it at 180 °C for 60 s, then dissolved PMMA with acetone, found that monolayer graphene curled into CNSs. This curling degree is related to the interactions between graphene and the SiO_2/Si substrate [48]. Currently, Schmidt et al. reported a well-controlled approach to form electrically contacted, suspended CNS by exploiting the spontaneous edge rolling of suspended GNRs with large length to width aspect ratio. Van der Waals interaction between the overlapping layers fixes the nanoscroll once formed. The stability of these CNSs was investigated by helium nano ion beam assisted in situ cutting [49]. The prepared CNSs have a perfect crystal structure,with few defects because this method is based on mechanically exfoliated monolayer graphene as

precursor, but the production rate is low, and it is not suitable for large-scale industrial production, and is only used in basic research in laboratory.

3.2.2 Freeze-drying strategy

Molecular dynamic simulations show that temperature is a key dominant factor for the stability of CNSs [50]. Controlled lyophilization of chemically reduced graphene oxide (CRG) is considered to be a simple and high effcient method to prepare CNSs in large scale. Usually, low concentration of precursor is prerequisite to reach a high transformation effciency of CNSs from graphene oxide (GO) sheets [51]. Xu et al. proposed a well controlled lyophilization method to transform scalable giant GO sheets to neat CNSs in high efficiency up to the yield of 92%. It comprises four sequential steps: chemical reduction of giant GO, freezing isolation of reduced graphene sheets, freeze-drying, and thermal annealing. Among these procedures, freeze-drying is one of the most important steps for forming the CNSs. The sublimation of ice made CRG sheets become freestanding, and these freestanding parts began to scroll. This tendency was exhibited by the rolling fringes of CRG sheets and CNSs at the surface of ice. It can be deduced that the scrolling of CRG sheets was driven by the sublimation of ice and free-standing of CRG sheets, And futher concluded that the topological scrolling is dominated by three factors: the chemical reduction, concentration of feed CRG dispersions, and freezing rate. The chemical reduction enhances the van der Waals force interaction of the CRG sheet to overcome the energy barrier of scrolling. The low concentration and fast freezing isolate CRG sheets in ice, keeping them free from contacting each other. In the following freeze-drying, the sublimation of ice induces the isolated CRG sheets to freely roll to scrolls [31]. Subsequently, N-doped 3D CNSs-based foam was synthesized using FA molecules as auxiliary cross-linking reagent under a mild heating process at 90 °C (formation of hydrogel with cross-linked GO sheets) and subsequent freeze-drying treatment (formation of aerogel with GO sheets rolling up into CNSs) [51]. On the basis of this mechanism, Zuo et al designed a 1D tubular structure of reduced graphene oxide (RGO)/S nanoscroll materials (denoted as RGO/SNS) by an environmentally friendly freeze-casting strategy without any toxic organic solvents in Fig. 6. In this method, the dispersion of prepared RGO and sulfur nanoparticle was cold-quenched with liquid nitrogen, followed by a freezedrying and heat-treatment process. In this unique architecture, the sulfur was encapsulated into the cavities of RGO nanoscrolls [52]. Jin et al. prepared RGO-poly-(2-(dimethylamino) ethyl methacrylate)-Pt/Ag nanoscrolls through a lyophilization method [53]. Freezing rate was also demonstrated to be a important factor dominating the topological transformation.

3.2.3 Cold quenching

When the heated carbon materials are dipped into the low-temperature solution, the temperature of the surface comes down immediately, while the internal temperature is still very high. The power necessary for the nanosheets to crimp is then produced. Figure 7 shows that a graphite rod was rapidly heated to red-hot (800 °C) in air, and then quickly dipped it into cold water (0 °C). The two processes were repeatedly performed for several times, then many CNSs

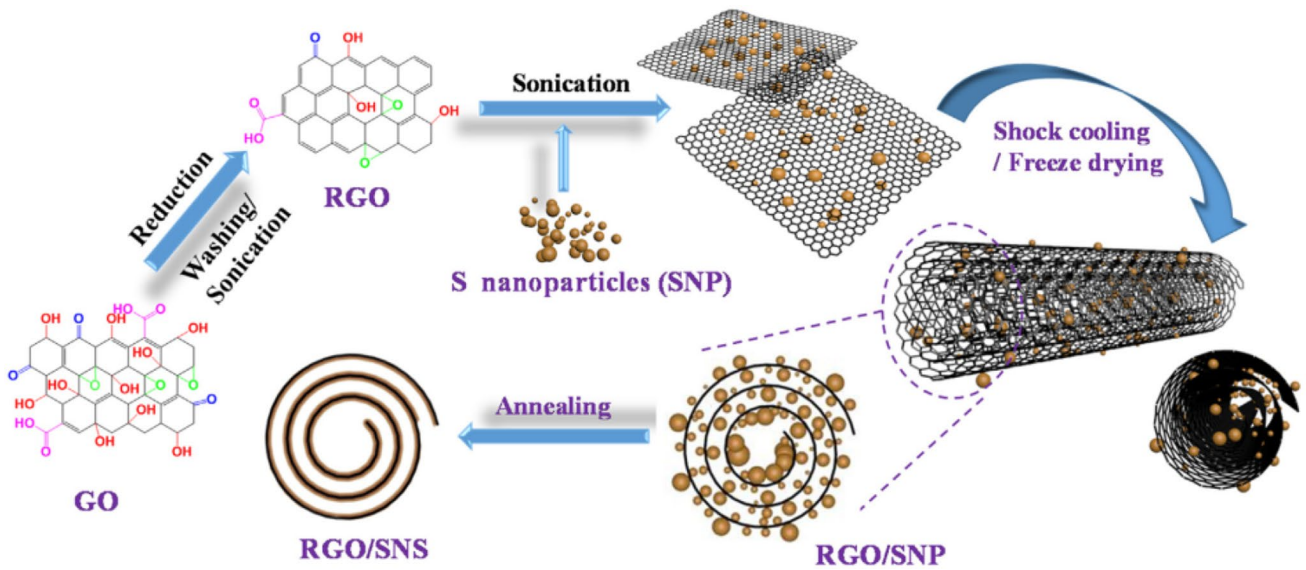

Fig. 6 Schematic diagram of the fabrication process of RGO/SNP and RGO/SNS. Reproduced from Ref. [52]. Copyright 2016 Elsevier Ltd

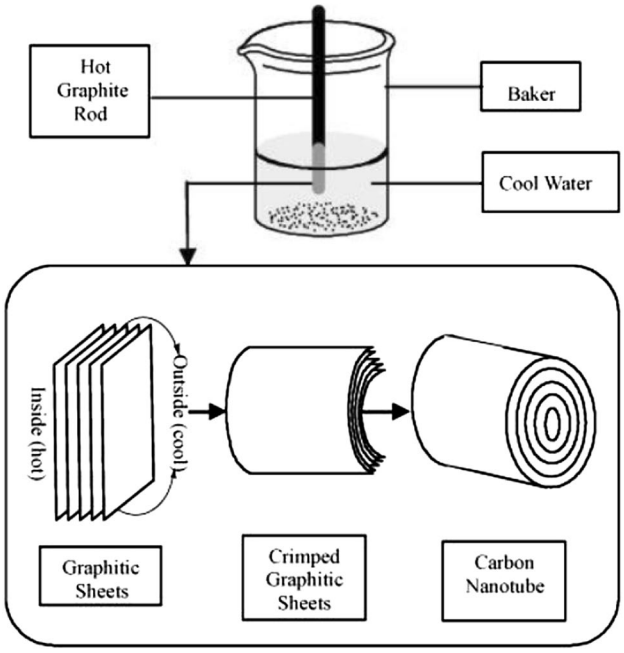

Fig. 7 One-step water-assisted synthesis of high-quality CNSs directly from graphite. Reproduced from Ref. [54]. Copyright 2003 American Chemical Society

were synthesised [54]. According to the estimation, the CNSs yield reaches about 40%. It can be found that The CNSs have the diameters in the range of tens and the lengths in the range of hundreds of nanometers. The inner diameters are between 5 and 10 nm, and the outer diameters are between 30 and 50 nm. The Raman spectroscopy shows that ID/IG = 0.05, which indicates the resulting CNSs have excellent crystal structure, with no defects, and no pollutions at the edge or on the surface.

Because GO surface contains many defects and oxygen-containing functional groups, in order to make GO nanosheets roll up, it is necessary to further reduce the reaction temperature. So the 1D graphene nanoscrolls was synthesized by rapid quenching of aqueous suspension of chemically reduced graphene using liquid nitrogen by Mohanapriya et al. [55] and Gao et al. [56], respectively. Zhao et al. developed a novel and simple method for the large-scale preparation of Fe_3O_4@CNSs from GO sheets by cold quenching in liquid nitrogen. During the cold quenching process, GO sheets are able to roll up into CNSs and the Fe_3O_4 nanoparticles also intercalate in the interlayer galleries of GNSs [57]. The key steps for preparation Fe_3O_4@CNSs materials is cold quenching by liquid nitrogen (Fig. 8). The mixed suspension of GO and Fe_3O_4 nanoparticles in a plastic box was heated up to 80 °C, the plastic box with the hot GO suspension was put into liquid nitrogen quickly for cold quenching. The structural conversion is closely correlated with the initial temperature of mixed suspension, the zeta potential of Fe_3O_4 nanoparticles and the immersion way. Sebsequently, a series of Fe_3O_4@CNSs with different Fe_3O_4/GO ratios were prepared by cold quenching of the mixed suspensions of Fe_3O_4 nanoparticles and GO in liquid nitrogen followed by thermal reduction [58]. More recently, the Fe_3O_4@CNSs-CNTs composites were obtained by cold quenching of GO and nickel acetate, CNSs-CNTs through CVD and heat treamentin Ar atmosphere [59]. Due to the increase of surface stress which is caused by the transport and removal of water during the ice crystal growing process, the GO sheets turn into nanoscroll structure and the adsorbed ions are wrapped simultaneously during the rolling process. Zhang et al. reported that the nanoscroll/nanosheet hybrid aerogels (GNAs) with confined SnS_2 nanosheets were facilely prepared via fast quenching, freeze-drying and thermal annealing. During quenching, wrapping SnS_2 nanosheets in the nanoscrolls and bridging the one-dimensional nanoscrolls by the two-dimensional nanosheets occur simultaneously, and the ratio of nanoscrolls/nanosheets can be controlled by simply adjusting quenching conditions. They further explained how a GO nanosheet is transformed into a GO nanoscroll in liquid nitrogen. The thin edges and corners of the GO sheet curl first to accommodate the strong

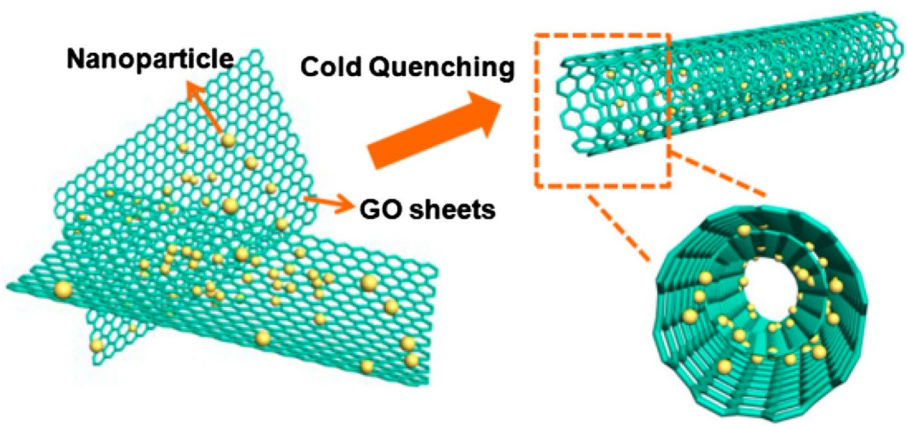

Fig. 8 Schematic diagram of synthetic route of Fe_3O_4@CNSs composite. Reproduced from Ref. [57]. Copyright 2014 American Chemical Society

cooling effect caused by the huge temperature change. The resultant surface strain along with the rapid bubbling caused by the heat released from the GO nanosheets then induce self-assembly of 2D nanosheets into 1D nanoscrolls [60].

3.3 CNSs prepared by surface modification

3.3.1 Functional groups modification on graphene surface

It is worth mentioning that the huge increase in the number of research projects aimed at functionalization of graphene including reactions of graphene (and its derivatives) with organic and inorganic molecules, chemical modification of the large graphene surface, and the general description of various covalent and noncovalent interactions with graphene [61]. So this technique was gradually applied to the preparation of CNSs.

Zhu et al. demonstrated the scrolling of graphene that is partially hydrogenated on one side, using molecular dynamics simulations. If a proper size of the graphene is hydrogenated on one side, the graphene can completely scroll up into a CNS that remains stable at room temperature.The curling up and scrolling of the hydrogenated region of the graphene is due to the accumulated effect of the local lattice distortion in the graphene at each adsorbed hydrogen atom [62].

GO can be easily converted into its graphene analog by chemical reduction, and is easy to covalently conjugate by reaction with functional groups at its basal plane and edges [63, 64]. So Kim et al. converted the carboxylic acid groups at the edges of the GO sheets to acid chlorides. Then, let it reflux with aminated CNTs at 120 °C for 5 days to prepare CNSs (as shown in Fig. 9). The formation mechanism can be summarized as follows: firstly, the carbonyl chloride groups at the edge of the GO react with amine groups on the surface of a MWCNT to form amide bonds, which anchor the GO sheets on the surface of MWCNTs. Secondly, the anchored GO sheets curve along the surface of the MWCNTs due to shear stress from vigorous stirring and continuous perturbation of the surrounding solvent. Finally, the curved GO sheets form scrolls around the surface of the aminated MWCNTs. Despite the higher energy of the curved GO conformation, scroll formation decreases the total free energy of GO due to attractive interaction between the oxygen containing reactive functional groups on the basal plane of the GO and the amine groups on the surface of the MWCNTs [65]. This preparation method produces uniform sized nano-materials, with controllable number of dimensions. However, the reaction processes may be too complex and the reaction time is too long [66] (Fig. 10).

3.3.2 Nanoparticles modification on graphene surface

The oxygen-containing functional groups (carboxyl, carbonyl, hydroxyl, and epoxide) existed on the surfaces of GO, which can act as the active sites for the trapping, stabilization, and nucleation of the metal ions. When the precursor solution of metal oxide or metal particles is gradually added into the GO suspension, the metal oxide or metal particles can be trapped by the oxygen-containing functional groups and start to grow into clusters on the surface of the GO sheet.

Wang et al. demonstrated an efficient and controllable way to roll up GO sheets into micro/nanoscrolls. The rolling process is highly enhanced by nanoparticle aggregation. Nanoparticles like Ag or Fe_3O_4 attached onto GO sheets can help the rolling process, which may be expected to expand into other inorganic nanoparticles [67]. Moreover, Sharifi et al. reported a 100% efficient process to transform nitrogen-doped reduced graphene oxide (N-RGO) sheets into homogeneous nanoscrolls by decoration with magnetic gamma-Fe_2O_3 nanoparticles. The rolling is initiated by the strong adsorption of maghemite nanoparticles at nitrogen defects in the graphene lattice and their mutual magnetic interaction. The nanoscroll formation is fully reversible and upon removal of the maghemite nanoparticles, the nanoscrolls return to open sheets. The strong dipole moment of maghemite nanoparticles and their strong interaction with the nitrogen functionalities on the N-RGO are the two most important causes to initiate the formation of the nanoscrolls. The maghemite formation requires the support of nitrogen defects on the graphene sheets and the solution PH has a significant role in directing the iron oxide crystallization towards maghemite instead of hematite. And water, besides

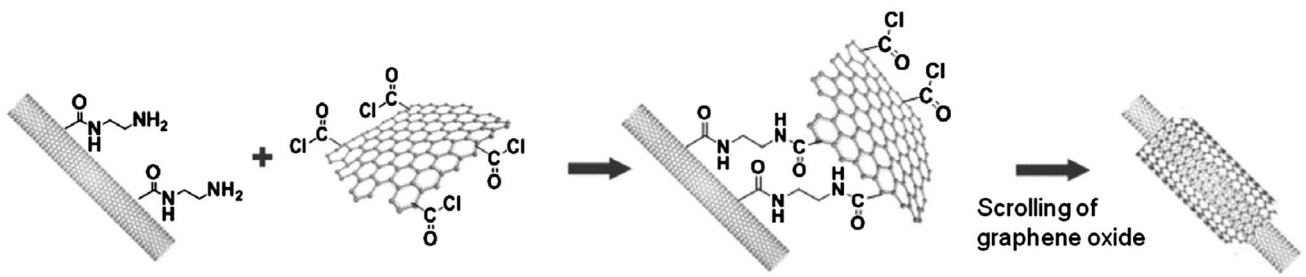

Fig. 9 Preparation of scrolls graphene oxides with MWCNTs templates. Reproduced from Ref. [65]. Copyright 2010 Elsevier Ltd

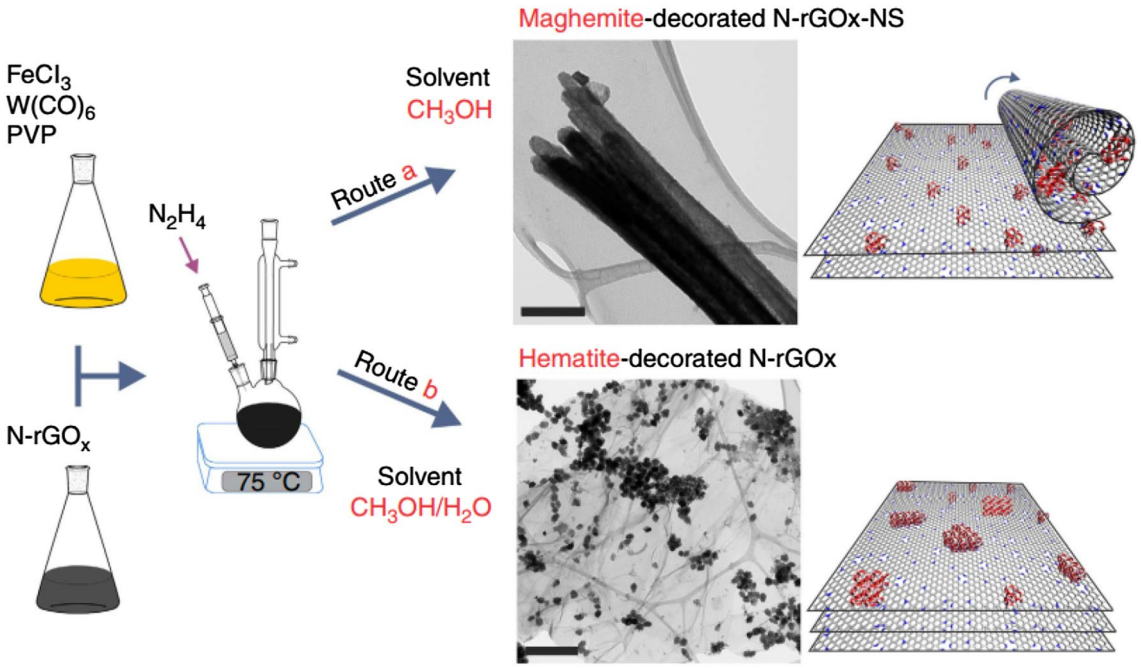

Fig. 10 Schematic process for the adsorption of iron oxide nanoparticles. (route a) Maghemite-decorated N-RGO nanoscrolls, and (route b) hematite-decorated N-RGO sheets. Reproduced from Ref. [68]. Copyright 2013 Macmillan Publishers Limited

balancing the pH to more neutral condition, also could have other roles in the ordering of the hematite nanoparticles, for example, altering the molecular arrangement of methanol. This can affect the polarity and size of methanol/water clusters, which are important for the solvation forces between a colloidal particle and the solvent, and therefore also vital in the nanoparticle formation/aggregation [68].

3.4 CNSs caused by mechanical force

3.4.1 Mechanical ball milling method

Mechanical ball milling is a low-cost, high yield and promising material preparation method [69, 70]. During the process of mechanical ball milling, materials deformation, fracture and cold welding occur, and patticles are constantly refined [71]. The unreacted surface is constantly exposed, which increases the contact area of the reaction, shortens the diffusion distance at the same time, the introduction of a large number of micro defects, such as dislocations and interface, significantly reduces the element diffusion activation energy, and provides fast diffusion channels, so as to improve the effect of diffusion reaction. Zhao et al. successfully prepared less than three layers of graphene by ball-milling graphite nanosheets into DMF for 30 h [72]. Chen et al. changed the ball milling process, they conducted mechanical ball-milling of graphite powder for 200 h in argon atmosphere, and then performed calcination at 1400 °C in argon atmosphere, the CNSs with external diameter of 4–20 nm and internal diameter of 1.8 nm were synthesised [73]. The authors further clarified that the calcination temperature (1400 °C) is far lower than the crystallization temperature (2000 °C) of amorphous carbon, and surface diffusion is the most possible formation mechanism of CNSs [74]. After that, Li et al. further improved the preparation process and directly conducted ball-milling using GN2 high energy ball-milling machine in Ar atmosphere, resulting in the formation of CNSs. The diameter of CNSs is 80–400 nm, the length is several nanometers. After calcination at 1800 °C for 0.5 h, the morphology of CNSs remains unchanged [75]. Although this method is simple and lower-cost, it can not completely peel off graphite, most of which are multilayer structure.

3.4.2 Ultrasound-assisted synthesis

It is worth noting that the numerous methods to produce graphene and graphene-derived compounds involve the use of sonication (more precisely ultrasonication) as an important, often key, experimental step. The effects of ultrasound on materials are in principle well established and two major contributions arise from cavitation and shear forces [76]. So sonication often causes the nanosheet scrolling or deformation.

Due to the weak van der Waals force between graphite layers, some small substances (K, Na, HNO_3, H_2SO_4) can be intercalated into graphite layers and then subjected

to ultrasonic oscillation, the exfoliated graphite sheets curl onto themselves, forming CNSs. Figure 11 presents that layered graphite can readily be intercalated using alkali metals, and forms the intercalation compound, upon sonication, the exfoliated graphite sheets curl onto themselves, forming CNSs [77]. This method is simple and effective. According to TEM osbervation with copper mesh, 80% of graphite sheets are rolled up, the forming CNSs consisting of 40 ± 15 layers of single-layer graphene, with interlayer spacing of 0.34 nm and diameter of 40 nm by average.

On this basis, Shioyama and Akita made certain improvements. They also firstly prepared KC_8, and then reacted KC_8 with unsaturated alkane (isoprene, styrene, etc.), subjected to NMP to remove organics and form CNSs [78]. The resulting CNSs have a open top, which consist of 15 graphene layers, with internal and external diameter of 16 nm and 26 nm, respectively. One of the most significant factors which determine the diameter of CNSs is the balance between surface energy decrease and bending energy increase. After that, more oxidizers were used for synthesis of graphite intercalation compounds ($K_2Cr_2O_7$, CrO_3, $KMnO_4$, etc.) [79, 80], such method can be extended to large-scale production, the intercalation destroys the original sp^2 structure of graphene, making impact to the physical and chemical properties of CNSs, but the use of O_3 can avoid carbon materials pollution. After completing the reaction the resulting suspension of exfoliated graphite in ethanol was sonicated and the CNSs were consisted of 15–20 of single-layer graphene, with diameter of 40–120 nm, length of 750 nm were formed [81].

3.4.3 Langmuir–Blodgett method

Langmuir–Blodgett (L–B) technology is a single molecular membrane deposition technique, which can accurately control membrane thickness and molecular arrangement, it can arrange insoluble film-forming material molecular in compact and orderly pattern at air–water interface for forming monomolecular film, and then transfer it to solid substrate. Gao et al. applied L–B technique in preparation of CNSs. The authors first prepared GO by improved Hummers method using natural flake graphite as raw materials, and then reacted GO with octadecylamine (ODA) to synthesize ODA-GO. Then, the ODA-GO was dissolved into methylbenzene for ultrasonic dispersion, followed by centrifugation to remove supernate, and subjected to L–B compression (Fig. 12). After compression, some hollow tubulous nanowires were formed near screen zone, with uneven tube walls. The length of CNSs prepared by L–B method is larger than 200 μm, which is much longer than the horizontal dimension of a single ODA-GO. This indicates such structure is probably formed by arrangement of single CNS in linear edge to edge and head to head pattern [82].

4 Applications of carbon nanoscrolls

Since the discovery of CNTs in 1991 and the successful preparation of single-layer graphene in 2004, they have attracted extensive attentions due to their excellent electrical and thermal conductivity as well as good mechanical properties, and have been used in the field of lithium ion batteries [57, 83, 84], supercapacitors [85], sensors [86],

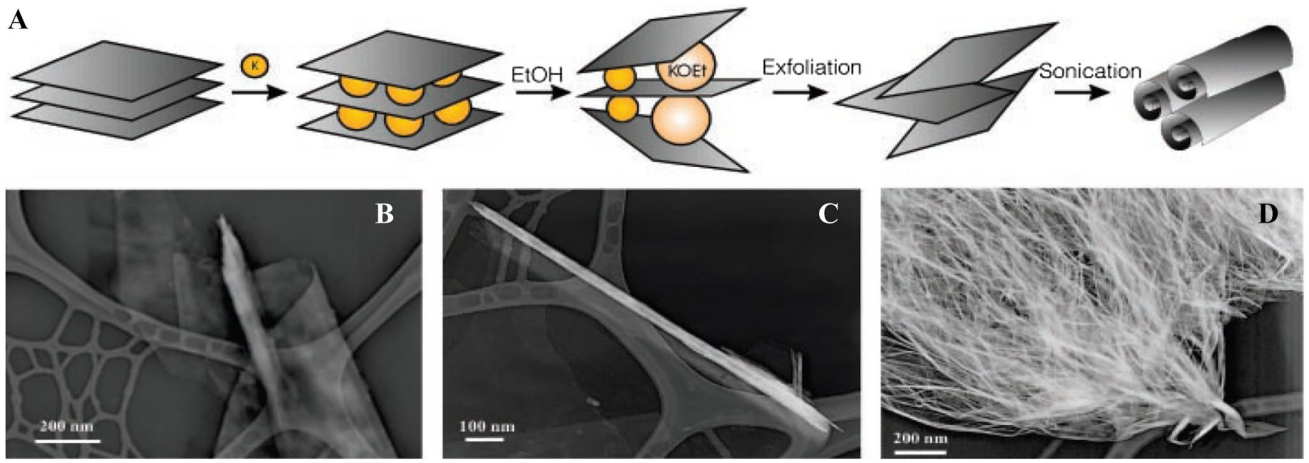

Fig. 11 A chemical route to CNSs. **a** Schematic of the intercalation/exfoliation process. Graphite is intercalated with potassium metal and then exfoliated with ethanol (EtOH) to form a dispersion of carbon sheets. Sonication produces CNSs. TEM images of **b** a thin plate of graphitic sheets in the process of scrolling, **c** an isolated carbon nanoscroll with open ends, and **d** a mass of scrolled material, representative of the bulk of the sample. The lighter web pattern in the background of each image is the lacey carbon TEM grid. Reproduced from Ref. [77]. Copyright 2003 Science

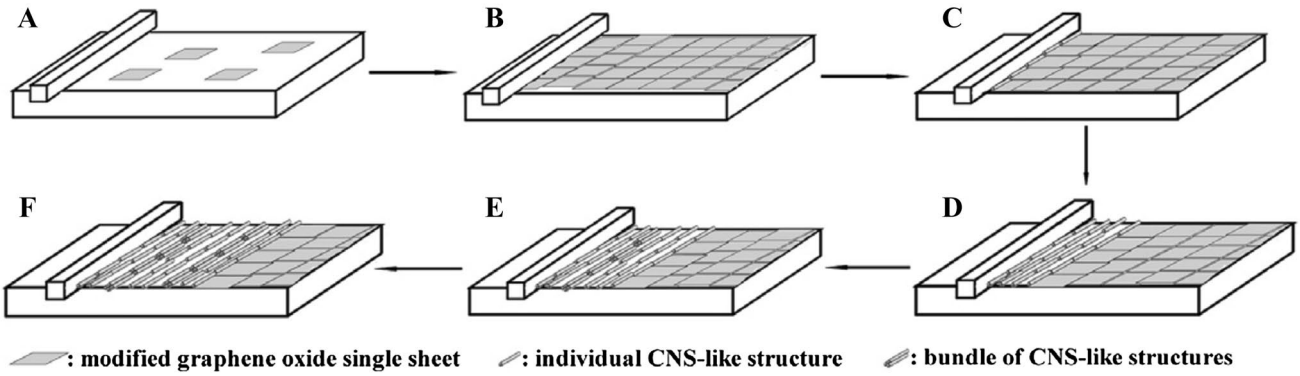

Fig. 12 Schematic representation of the formation of CNSs-like structures and the loose-dense pattern during L–B process. Reproduced from Ref. [82]. Copyright 2010 Elsevier Ltd

solar panels [87], transistors [88], ionic sieve [89], drug controlled release [90], and other composite materials [91]. CNSs are a 1D CNT-like nanomaterials made by rolling up 2D graphene, which have the properties of 1D CNTs and 2D graphene as well as theirs own unique electrical [92, 93], optical [94], mechanical [95, 96], elastic [97], magnetic [98] and quantum transport [99] properties. Therefore, the CNSs are expected to applied in more technical fields.

4.1 Lithium ion/sulfur batteries

Compared with CNTs, CNSs provide open structure at both ends and interlayer galleries that can be easily intercalated and adjusted [57]. V_3O_7 nanowire/CNSs composites exhibit an optimal performance with specific capacity of 321 mA h g^{-1} at 100 mA g^{-1} and 87.3% capacity retention after 400 cycles at 2000 mA g^{-1} [100]. TiO_2 (B) nanowires/CNSs hybrids remain 153 mA h g^{-1} after 300 cycles at 10 °C with capacity retention of 94% [83]. Graphene nanoscroll-wrapped of Fe_3O_4 nanoparticles show excellent cycling stability with a reversible capacity of 1172 mA h g^{-1} over 200 cycles at 100 mA g^{-1} and 525 mA h g^{-1} over 1000 cycles at 2 A g^{-1}, as well as superior rate performance with a reversible capacity of 648 and 480 mA h g^{-1} at 2 and 5 A g^{-1}, respectively [58]. As anode materials for lithium ion batteries, MnO_2 nanowire/CNSs composites [100], carbon capsulated SnO_2@CNSs/TiO_2 composites [101], SnS_2 nanosheets/CNSs composites [60] also exhibit outstanding Li-ion storage characteristics. When it is used as a cathode material for lithium–sulfur batteries, the sulfur/RGO nanoscrolls exhibit high initial capacity of 1295 mA h g^{-1} and reversible capacity of 744 mA h g^{-1} after the 100th cycle at 0.2 °C [102]. The remarkable electrochemical performance of the sulfur/RGO nanoscroll materials is mainly attributed to the desirable structural features, where sulfur is encapsulated into the RGO nanoscrolls and kept close contact with RGO [52]. These excellent energy storage capacities and cycling performance are attributed to the unique structure of the CNSs, which provides continuous electron and ion transfer channels and space for free volume expansion of nanowires during cycling.

4.2 Fuel cells

The primary demands on the hydrated proton exchange membrane are high proton conductivity, low fuel and oxygen permeability, and high chemical, thermal and mechanical stability. In view of this characteristic, the Nafion/CNSs composite membrane was prepared for proton exchange membrane fuel cells by Feng et al., the resultant composite membrane exhibits excellent proton conductivity compared to that of the recast Nafion membrane, especially under low-humidity conditions. It is mainly attributed to the rearrangement of the microstructures of Nafion matrix by CNSs to significantly facilitate the proton transport [103]. Subsequently, Liu et al. synthesized the Pt/RGO nanoscrolls catalyst. The electrocatalytic performance of the Pt/RGO nanoscrolls for methanol oxidation was evaluated, and the results show that the high surface area and porous structure of CNSs effectively avoid the migration and falling of Pt NPs in the methanol electrooxidation process, resulting in the high electrocatalytic mass activity and long-term stability of Pt/CNSs [104].

4.3 Supercapacitors

Supercapacitors, as an intermediate system between dielectric capacitors and batteries, have drawn significant attention due to their superb characteristics of high power density and long cycle life. So far, various materials have been used as electrode materials for supercapacitors. But their capacitance properties have not reached the expected standard. The unique scrolled characteristics of CNSs are favorable for the electrode materials to contact the electrolyte and form the

double electric layer capacitors between the layers. Therefore, CNSs were successfully applied to supercapacitors by Zeng et al. [105], compared with the specific capacity of 110 F g^{-1} for graphene sheets, a remarkable capacity of 162.2 F g^{-1} is obtained at the current density of 1.0 A g^{-1} in 6 M KOH aqueous solution owing to the unique scrolled structure of graphene scrolls. The capacity value is increased by about 50% only because of the topological change of graphene sheets. Meanwhile, CNSs exhibit excellent long-term cycling stability along with 96.8% retained after 1000 cycles at 1.0 A g^{-1}. Subsequently, Mohanapriya's experimental results show that the specific capacitance of 309.8 F g^{-1} for CNSs at the constant current density 0.5 A g^{-1}. The maximum energy and power densities achieved for GNS are 27.5 Wh kg^{-1} and 10,800 W kg^{-1}, respectively with excellent cyclic stability [55]. Moreover, Co_3O_4-reduced GO scrolls was fabricated for high-performance supercapacitor electrodes [106], the Co_3O_4/CNSs composites show a slightly better retention of 93% than that of Co_3O_4 (91%) after 1000 cycles. Subsequently, Zheng et al. growed polyaniline on graphene nanoscroll composites. The best specific capacitance of the composites reach 320 F g^{-1} at 1 A g^{-1} and a 92.1% retention capacitance rate is obtained at 100 A g^{-1} [107], indicating that the polyaniline/CNSs composites have a rate performance as good as CNSs and a higher specific capacitance. These extraordinary electrochemical properties could be attributed to the unique tubular 1D morphology of CNSs with open ends/edges. These outcomes illustrate that the unique topology of CNSs would possess new future electrode material for next generation supercapacitors.

4.4 Hydrogen storage

Hydrogen is considered the best potential successor to gasoline due to its clean combustion. When it burns it only produces water. Braga and Mpourmpakis respectively reported the hydrogen storage ability of CNSs. Braga et al. found that storing hydrogen at low temperature is possible, while high temperature may reduce its capacity, making small part of hydrogen stored in CNSs [108]. Mpourmpakis et al. from Greece calculated the potential parameter of interaction between hydrogen and CNS wall, and then conducted Monte Carlo simulation, finding that pure CNSs could not store hydrogen because of the small interlayer spacing, while a helical nanoscroll (0.7 nm) with intercalation of alkali metals is the ideal material to store hydrogen [27]. Subsequently, Huang et al. studied the transportation properties of hydrogen atoms through the CNSs by comprehensive molecular dynamics simulations. The CNSs are slightly deformed and tilted towards the end of the simulation, which attribute to the strain energy induced by the interaction between hydrogen atoms absorbed and the inner layer of CNSs. Hydrogen atoms are more easily transported through the CNSs instead of being trapped, with a higher pumping speed [109].

4.5 Sensors

The CNSs are suitable for nanoscale applications such as in nanotransistors, and biosensor devices due to theirs 1D structure and tunable core size. An analytical model of liquid-gated field effect transistors (LGFETs) for zig-zag graphene nanoscrolls inspired by carbon nanotube behavior when exposed to DNA molecules was established by Karimi et al. [86]. Based on the sensing mechanism of the DNA sensor, CNSs controlling elements are proposed and the behavior of LGFETs-based CNSs nanomaterial in the presence of DNA molecules is predicted to get a greater insight into the rapid development of DNA sensors and their application. Recently, platinum nanoparticles/nitrogen doped graphene nanoscrolls (Pt/N-GSS) nanocomposites were prepared as new amperometric glucose biosensor [110]. Based on the fantastically scrolled structure, N-doping and high reduction degree properties of N-GSS as catalyst support for Pt nanoparticles, Pt/N-GSS nanocomposites exhibit excellent electrocatalytic activity towards the oxidation of H_2O_2 with the sensitivity of 25.26 mA mM^{-1} and good linear response from 2 to 16.57 mM. Moreover, molecular combing is utilized to fabricate well-aligned GO scrolls with high yield on hydrophobic substrates. As a proof of concept, A gas sensor based on a single RGO scroll was fabricated, which was successfully used to detect NO_2 gas with concentration as low as 0.4 ppm [111].

4.6 Oscillators

The oscillator is an electronic circuit that produces a periodic, oscillating electronic signal, often a sine wave or a square wave. Oscillators convert direct current from a power supply to an alternating current signal. They are widely used in many electronic devices. Shi et al. performed theoretical study and molecular dynamics simulations to investigate the gigahertz "breathing" oscillatory motion of a CNS [112]. It is shown that the oscillation frequency depends on surface energy, bending stiffness, interlayer spacing, and length of the basal graphene sheet of the CNSs, and that energy dissipation in the system can be controlled by adjusting temperature, graphene length, and surface energy. Subsequently, the ultrafast axial nano-oscillators were fabricated based on CNSs using molecular dynamics simulations by Zhang et al. [113]. CNSs-based nano-oscillator can be excited and driven by an external AC electric field, and oscillate at more than 100 GHz. Besides that, Cheng et al. also demonstrated a substrate-supported CNSs oscillator through MD simulations [114]. The motion of such an oscillator on substrate is guided and can be controlled, which may offer a unique

advantage over other types of oscillators. The substrate-supported CNSs oscillator requires a sufficiently rigid insertion to constrain its core during oscillation, and the elastic property of the insertion influences the oscillatory behavior of the CNSs. The CNS-based nano-oscillators not only offer a feasible pathway toward ultrafast nano-devices but also hold promise to enable nanoscale energy transduction, harnessing, and storage.

4.7 Photocatalytic materials

Recent reports [115–117] present that the photocatalysts prepared in conjunction with graphene, due to its outstanding mechanical, electrical, surface and optical properties and good interfacial contact with adsorbents. But graphene is easy to agglomerate, and its performance can not be fully achieved. So Li et al. prepared potassium niobate/RGO composite nanoscrolls [118]. With CNSs as electron collector and transporter, the composite shows higher photocatalytic activity for the degradation of Rhodamine B (RhB). The synergistic effects of adsorption of RhB on catalyst surface and efficient charge separation play significant roles for degradation of RhB under UV irradiation. It is indicated that the potassium hexaniobate/RGO composite nanoscrolls are excellent candidates for applications relating to a number of environmental issues.

4.8 Other applications

CNSs have been widely used in the above fields because of their superior performance. Theirs theoretical simulation shows that they also have great potential in translational nanoactuator [30, 119], gas separation fields [120, 121], motors [119], microjet engines [122], water channels [123], drug-delivery systems [23, 124] and thermal interface materials fields [125]. Recently, Tarabkova [126] informs about the first experimental verification of so far only theoretically anticipated CNSs electro-nanoactuation. As the nanoactuation that is driven by low voltage in aqueous electrolyte solution, it indicates also the prospective utilization of nanoscroll as an electromechanical nanoactuator in biomedical applications.

5 Conclusions and outlook

CNSs, a rapidly rising star of carbon family, is a spirally wrapped 2D graphene sheet with 1D tubular but open topological structure, differing from the seamless concentric structure of MTCNTs. The spiral structure of CNSs with open edges and ends can help prevent the restacking of graphene substrates. Furthermore, CNSs possess highly adjustable interlayer distance and developed tunnel system, which renders foreign molecules to easily and continuously diffuse into their interlayer galleries without any limitation, because it can facilitate the radial expansion to accommodate the consecutive intercalation process.

In general, the quality of CNSs not only depends on the selection of the preparation methods, but also on the origin, size, thickness and surface defects of the precursor graphene. Commonly, CNSs prepared by chemical method have high yield, but the quality is poor, CNSs prepared from the physical technique, the precursor is mechanically exfoliated monolayer graphene, so it can achieve high quality, but theirs output are too low. In addition, currently, the preparation of CNSs is always qualitative research. It is just a simple study that By what method, how about the output of CNSs. The effects of graphene size, thickness, surface defects and other factors on the formation of CNSs have not been thoroughly investigated. There is few research on whether there is correlation between the different uses of CNSs and their specific layers. These will be one of the future development direction.

At present, although CNSs have been applied to energy storage, sensors, oscillators and other fields, most of them still remain in the laboratory and theoretical research stage, and their application areas need further expansion and there is still a long way to go for their industrialization. However, we believe that CNSs will become another bright star after CNTs and graphene in the foreseeable future.

Acknowledgements This work is financially supported by the National Natural Science Foundation of China (Grant No. 31671939), the Open Project Program from Chongqing Key Laboratory of Micro/Nano Materials Engineering (Grant No. KF201604), Technology and Basic and Frontier Research Program of Chongqing Municipality (Grant No. cstc2018jcyjAX0701) and (Grant No. cstc2017jcyjAX0326), and Major Program of Chongqing University of Arts and Sciences (Grant No. P2017XC06).

References

1. K.S. Novoselov, A.K. Geim, S.V. Morozov, D. Jiang, Y. Zhang, S.V. Dubonos, I.V. Grigorieva, A.A. Firsov, Science **306**, 666–669 (2004)
2. F.G. Brunetti, H. Isla, J. Arago, E. Orti, E.M. Perez, N. Martin, Chemistry **19**, 9843–9848 (2013)
3. J. Annett, G.L.W. Cross, Nature **535**, 271–275 (2016)
4. Y. Zhu, S. Murali, W. Cai, X. Li, J.W. Suk, J.R. Potts, R.S. Ruoff, Adv. Mater. **22**, 3906–3924 (2010)
5. A.A. Balandin, S. Ghosh, W. Bao, I. Calizo, D. Teweldebrhan, F. Miao, C.N. Lau, Nano Lett. **8**, 902–907 (2008)
6. C. Lee, X. Wei, J.W. Kysar, J. Hone, Science **321**, 385–388 (2008)
7. A.S. Mayorov, R.V. Gorbachev, S.V. Morozov, L. Britnell, R. Jalil, L.A. Ponomarenko, P. Blake, K.S. Novoselov, K. Watanabe, T. Taniguchi, A.K. Geim, Nano Lett. **11**, 2396–2399 (2011)
8. P. Suvarnaphaet, S. Pechprasarn, Sensors (Basel, Switzerland) **17**, 1–24 (2017)
9. G. Gorgolis, C. Galiotis, 2d Materials **4**, 1–21 (2017)

10. J. Wu, W. Pisula, K. Muellen, Chem. Rev. **107**, 718–747 (2007)
11. A.K. Geim, K.S. Novoselov, Nat. Mater. **6**, 183–191 (2007)
12. J.L. Atwood, G.W. Gokel, Nature **354**, 354–355 (1991)
13. G. Zhong, R. Xie, J. Yang, J. Robertson, Carbon **67**, 680–687 (2014)
14. A. Perez, E. del Pino, L. Gyoergy, B. Cabana, G. Ballesteros, Tobias, Carbon **50**, 4450–4458 (2012)
15. A.E. Islam, P. Nikolaev, P.B. Amama, S. Saber, D. Zakharov, D. Huffman, M. Erford, G. Sargent, S.L. Semiatin, E.A. Stach, B. Maruyama, Nano Lett. **14**, 4997–5003 (2014)
16. D. Luxembourg, G. Flamant, D. Laplaze, J.L. Sauvajol, S. Enouz, A. Loiseau, Fuller. Nanotubes Carbon Nanostruct. **15**, 257–266 (2007)
17. R. Das Gupta, C. Schwandt, D.J. Fray, Carbon **70**, 142–148 (2014)
18. S. Ye, F. Wu, X.-R. Ye, Y. Lin, J. Nanosci. Nanotechnol. **9**, 2781–2794 (2009)
19. X.S. Li, H.W. Zhu, B. Jiang, J. Ding, C.L. Xu, D.H. Wu, Carbon **41**, 1664–1666 (2003)
20. A. Beitollahi, S. Pilehvari, M.A.F. Sani, H. Moradi, M. Akbarnejad, Ceram. Int. **38**, 3273–3280 (2012)
21. S. Manafi, H. Nadali, H.R. Irani, Mater. Lett. **62**, 4175–4176 (2008)
22. A. Taraghi Osguei, M.T. Ahmadian, M. Asghari, N.M. Pugno, Materials (Basel, Switzerland) **10**, 1–25 (2017)
23. Y. Cheng, L.D. Koh, F. Wang, D. Li, B. Ji, J. Yeo, G. Guan, M.Y. Han, Y.W. Zhang, Nanoscale **9**, 9181–9189 (2017)
24. P. Yadav, S. Warule, J. Jog, S. Ogale, Solid State Commun. **152**, 2092–2095 (2012)
25. T.D. Daff, S.P. Collins, H. Dureckova, E. Perim, M.S. Skaf, D.S. Galvao, T.K. Woo, Carbon **101**, 218–225 (2016)
26. Y. Wang, H.F. Zhan, C. Yang, Y. Xiang, Y.Y. Zhang, Comput. Mater. Sci. **96**, 300–305 (2015)
27. G. Mpourmpakis, E. Tylianakis, G.E. Froudakis, Nano Lett. **7**, 1893–1897 (2007)
28. R. Bacon, J. Appl. Phys. **31**, 283–290 (1960)
29. V.P. Dravid, X. Lin, Y. Wang, X.K. Wang, A. Yee, J.B. Ketterson, R.P.H. Chang, Science **259**, 1601–1604 (1993)
30. S.F. Braga, V.R. Coluci, S.B. Legoas, R. Giro, D.S. Galvao, R.H. Baughman, Nano Lett. **4**, 881–884 (2004)
31. Z. Xu, B. Zheng, J. Chen, C. Gao, Chem. Mater. **26**, 6811–6818 (2014)
32. N. Patra, B. Wang, P. Kral, Nano Lett. **9**, 3766–3771 (2009)
33. B.V.C. Martins, D.S. Galvao, Nanotechnology **21**, 75710 (2010)
34. V.B. Shenoy, C.D. Reddy, Y.-W. Zhang, ACS Nano **4**, 4840–4844 (2010)
35. Z. Zhang, T. Li, Appl. Phys. Lett. **97**, 283–288 (2010)
36. O. Zhou, R.M. Fleming, D.W. Murphy, C.H. Chen, R.C. Haddon, A.P. Ramirez, S.H. Glarum, Science **263**, 1744–1747 (1994)
37. A.R. Muhammad Musaddique, I. Javed, J. Encapsul. Adsorpt. Sci. **1**, 29–34 (2011)
38. M. Takizawa, S. Bandow, M. Yudasaka, Y. Ando, H. Shimoyama, S. Iijima, Chem. Phys. Lett. **326**, 351–357 (2000)
39. J.G. Lavin, S. Subramoney, R.S. Ruoff, S. Berber, D. Tomanek, Carbon **40**, 1123–1130 (2002)
40. B.A. Kakade, H. Allouche, S. Mahima, B.R. Sathe, V.K. Pillai, Carbon **46**, 567–576 (2008)
41. A.K. Schaper, H. Hou, M. Wang, Y. Bando, D. Golberg, Carbon **49**, 1821–1828 (2011)
42. A.L. Chuvilin, V.L. Kuznetsov, A.N. Obraztsov, Carbon **47**, 3099–3105 (2009)
43. J. Ning, D. Wang, Y. Chai, X. Feng, M. Mu, L. Guo, J. Zhang, Y. Hao, Nanotechnology **28**, 284001 (2017)
44. G. Cheng, I. Calizo, X. Liang, B.A. Sperling, A.C. Johnston-Peck, W. Li, J.E. Maslar, C.A. Richter, A.R.H. Walker, Carbon **76**, 257–265 (2014)
45. H. Liu, J. Huang, X. Li, J. Liu, Y. Zhang, J. Wuhan Univ. Technol.-Mater. Sci. Ed. **28**, 220–223 (2013)
46. X. Xie, L. Ju, X. Feng, Y. Sun, R. Zhou, K. Liu, S. Fan, Q. Li, K. Jiang, Nano Lett. **9**, 2565–2570 (2009)
47. Q. Li, Z. Li, M. Chen, Y. Fang, Nano Lett. **9**, 2129–2132 (2009)
48. H.Q. Zhou, C.Y. Qiu, H.C. Yang, F. Yu, M.J. Chen, L.J. Hu, Y.J. Guo, L.F. Sun. Chem. Phys. Lett. **501**, 475–479 (2011)
49. M.E. Schmidt, A.M.M. Hammam, T. Iwasaki, T. Kanzaki, M. Muruganathan, S. Ogawa, H. Mizuta, Nanotechnology **29**, 235605 (2018)
50. L.J. Yi, Y.Y. Zhang, C.M. Wang, T.C. Chang, J. Appl. Phys. **115**, 204307 (2014)
51. Q. Fang, X. Zhou, W. Deng, Y. Liu, Z. Zheng, Z. Liu, Small **13**, 68–124 (2017)
52. P. Zuo, W. Zhang, J. Hua, Y. Ma, C. Du, X. Cheng, Y. Gao, G. Yin, Electrochim. Acta **222**, 1861–1869 (2016)
53. X. Jin, X. Wang, Y. Zhang, H. Wang, Y. Yang, Int. J. Hydrogen Energy **43**, 13440–13449 (2018)
54. Z.H. Kang, E.B. Wang, L. Gao, S.Y. Lian, M. Jiang, C.W. Hu, L. Xu, J. Am. Chem. Soc. **125**, 13652–13653 (2003)
55. K. Mohanapriya, N. Jha, Appl. Surf. Sci. **449**, 461–467 (2018)
56. L. Gao, Z. Zhang, J. Zhao, J. Zhou, Z. Miao, W. Si, S. Zhuo, RSC Adv. **8**, 19164–19170 (2018)
57. J. Zhao, B. Yang, Z. Zheng, J. Yang, Z. Yang, P. Zhang, W. Ren, X. Yan, ACS Appl. Mater. Interfaces **6**, 9890–9896 (2014)
58. B. Yang, J. Zhao, J. Chen, M. He, S. Xu, RSC Adv. **5**, 57906–57911 (2015)
59. Y. Liu, A.H. Siddique, H. Huang, Q. Fang, W. Deng, X. Zhou, H. Lu, Z.P. Liu, Nanotechnology **28**, 465401 (2017)
60. Y. Zhang, C. Zhao, Z. Zeng, J.M. Ang, B. Che, Z. Wang, X. Lu, Electrochim. Acta **278**, 156–164 (2018)
61. V. Georgakilas, M. Otyepka, A.B. Bourlinos, V. Chandra, N. Kim, K.C. Kemp, P. Hobza, R. Zboril, K.S. Kim, Chem. Rev. **112**, 6156–6214 (2012)
62. S. Zhu, T. Li, J. Phys. D-Appl. Phys. **46**, 075301 (2013)
63. X. Sun, Z. Liu, K. Welsher, J.T. Robinson, A. Goodwin, S. Zaric, H. Dai, Nano Res. **1**, 203–212 (2008)
64. C. Hontorialucas, A.J. Lopezpeinado, J.D.D. Lopezgonzalez, M.L. Rojascervantes, R.M. Martinaranda, Carbon **33**, 1585–1592 (1995)
65. Y.K. Kim, D.H. Min, Carbon **48**, 4283–4288 (2010)
66. H.W. Liang, S. Liu, S.H. Yu, Adv. Mater. **22**, 3925–3937 (2010)
67. X. Wang, D.-P. Yang, G. Huang, P. Huang, G. Shen, S. Guo, Y. Mei, D. Cui, J. Mater. Chem. **22**, 17441–17444 (2012)
68. T. Sharifi, E. Gracia-Espino, H.R. Barzegar, X. Jia, F. Nitze, G. Hu, P. Nordblad, C.W. Tai, T. Wagberg, Nat. Commun. **4**, 1–9 (2013)
69. I.Y. Jeon, Y.R. Shin, G.J. Sohn, H.J. Choi, S.Y. Bae, J. Mahmood, S.M. Jung, J.M. Seo, M.J. Kim, D.W. Chang, L. Dai, J.B. Baek, Proc. Natl. Acad. Sci. USA **109**, 5588–5593 (2012)
70. X. Wang, G. Sun, P. Routh, D.-H. Kim, W. Huang, P. Chen, Chem. Soc. Rev. **43**, 7067–7098 (2014)
71. M. Khan, M. Amjad, A. Khan, R. Ud-Din, I. Ahmad, T. Subhani, J. Mater. Res. **32**, 2055–2066 (2017)
72. W. Zhao, M. Fang, F. Wu, H. Wu, L. Wang, G. Chen, J. Mater. Chem. **20**, 5817–5819 (2010)
73. Y. Chen, M.J. Conway, J.D. Fitz Gerald, Appl. Phys. A **76**, 633–636 (2003)
74. Y. Chen, M.J. Conway, J.D. Fitz Gerald, J.S. Williams, L.T. Chadderton, Carbon **42**, 1543–1548 (2004)
75. J.L. Li, Q.S. Peng, G.Z. Bai, W. Jiang, Carbon **43**, 2830–2833 (2005)
76. G. Cravotto, P. Cintas, Chemistry **16**, 5246–5259 (2010)
77. L.M. Viculis, J.J. Mack, R.B. Kaner, Science **299**, 1361–1361 (2003)
78. H. Shioyama, T. Akita, Carbon **41**, 179–181 (2003)

79. D. Roy, E. Angeles-Tactay, R.J.C. Brown, S.J. Spencer, T. Fry, T.A. Dunton, T. Young, M.J.T. Milton, Chem. Phys. Lett. **465**, 254–257 (2008)
80. F. Zeng, Y. Kuang, Y. Wang, Z. Huang, C. Fu, H. Zhou, Adv. Mater. **23**, 4929–4932 (2011)
81. M.V. Savoskin, V.N. Mochalin, A.P. Yaroshenko, N.I. Lazareva, T.E. Konstantinova, I.V. Barsukov, L.G. Prokofiev, Carbon **45**, 2797–2800 (2007)
82. Y. Gao, X. Chen, H. Xu, Y. Zou, R. Gu, M. Xu, A.K.Y. Jen, H. Chen, Carbon **48**, 4475–4482 (2010)
83. X. Li, Y. Zhang, T. Li, Q. Zhong, H. Li, J. Huang, J. Power Sources **268**, 372–378 (2014)
84. L. Mai, Q. Wei, Q. An, X. Tian, Y. Zhao, X. Xu, L. Xu, L. Chang, Q. Zhang, Adv. Mater. **25**, 2969–2973 (2013)
85. H. Wang, Q. Hao, X. Yang, L. Lu, X. Wang, Electrochem. Commun. **11**, 1158–1161 (2009)
86. H. Karimi, M.T. Ahmadi, E. Khosrowabadi, R. Rahmani, M. Saeidimanesh, R. Ismail, S.D. Naghib, E. Akbari, RSC Adv. **4**, 16153–16162 (2014)
87. H.A. Becerril, J. Mao, Z. Liu, R.M. Stoltenberg, Z. Bao, Y. Chen, ACS Nano **2**, 463–470 (2008)
88. A.Y. Kasumov, R. Deblock, M. Kociak, B. Reulet, H. Bouchiat, I.I. Khodos, Y.B. Gorbatov, V.T. Volkov, C. Journet, M. Burghard, Science **284**, 1508–1511 (1999)
89. K. Sint, B. Wang, P. Kral, J. Am. Chem. Soc. **130**, 16448–19449 (2008)
90. Z. Liu, J.T. Robinson, X. Sun, H. Dai, J. Am. Chem. Soc. **130**, 10876–10877 (2008)
91. D. Eder, Chem. Rev. **110**, 1348–1385 (2010)
92. Y. Chen, J. Lu, Z. Gao, J. Phys. Chem. C **111**, 1625–1630 (2007)
93. A.K. Schaper, M.S. Wang, Z. Xu, Y. Bando, D. Golberg, Nano Lett. **11**, 3295–3300 (2011)
94. T.S. Li, M.F. Lin, S.C. Chang, H.C. Chung, Phys. Chem. Chem. Phys. **13**, 6138–6144 (2011)
95. H.Y. Song, S.F. Geng, M.R. An, X.W. Zha, J. Appl. Phys. **113**, 164305 (2013)
96. T. Wang, C. Zhang, S. Chen, J. Nanosci. Nanotechnol. **13**, 1136–1140 (2013)
97. M.M. Zaeri, S. Ziaei-Rad, RSC Adv. **4**, 22995–23001 (2014)
98. L. Lai, J. Lu, L. Wang, G. Luo, J. Zhou, R. Qin, Y. Chen, H. Li, Z. Gao, G. Li, W.N. Mei, Y. Maeda, T. Akasaka, S. Sanvito, Nano Res. **2**, 844–850 (2009)
99. T.S. Li, M.F. Lin, Y.C. Huang, T.C. Lin, Phys. Lett. A **376**, 515–520 (2012)
100. M. Yan, F. Wang, C. Han, X. Ma, X. Xu, Q. An, L. Xu, C. Niu, Y. Zhao, X. Tian, P. Hu, H. Wu, L. Mai, J. Am. Chem. Soc. **135**, 18176–18182 (2013)
101. X. Li, Y. Zhang, T. Li, Q. Zhong, H. Li, J. Huang, Electrochim. Acta **147**, 40–46 (2014)
102. S. Yoo, J. Lee, J.M. Kim, C.-Y. Seong, K.-D. Seong, Y. Piao, J. Electroanal. Chem. **780**, 19–25 (2016)
103. K. Feng, B. Tang, P. Wu, ACS Appl. Mater. Interfaces **5**, 1481–1488 (2013)
104. Y. Liu, Y. Xia, H. Yang, Y. Zhang, M. Zhao, G. Pan, Nanotechnology **24**, 235401 (2013)
105. F. Zeng, Y. Kuang, G. Liu, R. Liu, Z. Huang, C. Fu, H. Zhou, Nanoscale **4**, 3997–4001 (2012)
106. W. Zhou, J. Liu, T. Chen, K.S. Tan, X. Jia, Z. Luo, C. Cong, H. Yang, C.M. Li, T. Yu, Phys. Chem. Chem. Phys. **13**, 14462–14465 (2011)
107. B.N. Zheng, C. Gao, New Carbon Mater. **31**, 315–320 (2016)
108. S.F. Braga, V.R. Coluci, R.H. Baughman, D.S. Galvao, Chem. Phys. Lett. **441**, 78–82 (2007)
109. J. Huang, C.H. Wong, Comput. Mater. Sci. **102**, 7–13 (2015)
110. L. Meng, Y. Xia, W. Liu, L. Zhang, P. Zou, Y. Zhang, Electrochim. Acta **152**, 330–337 (2015)
111. H. Li, J. Wu, X. Qi, Q. He, C. Liusman, G. Lu, X. Zhou, H. Zhang, Small **9**, 382–386 (2013)
112. X. Shi, N.M. Pugno, Y. Cheng, H. Gao, Appl. Phys. Lett. **95**, 163113 (2009)
113. Z. Zhang, T. Li, Nanoscale Res. Lett. **6**, 1–11 (2011)
114. Y. Cheng, X. Shi, N.M. Pugno, H. Gao, Physica E **44**, 955–959 (2012)
115. S. Pu, R. Zhu, H. Ma, D. Deng, X. Pei, F. Qi, W. Chu, Appl. Catal. B **218**, 208–219 (2017)
116. F. Li, B. Dong, Ceram. Int. **43**, 16007–16012 (2017)
117. R. Zhu, F. Tian, S. Che, G. Cao, F. Ouyang, Renew. Energy **113**, 1503–1514 (2017)
118. X. Li, T. Zhang, S. Gu, S.-Z. Kang, G. Li, J. Mu, Sep. Purif. Technol. **108**, 139–142 (2013)
119. X. Shi, Y. Cheng, N.M. Pugno, H. Gao, Appl. Phys. Lett. **96**, 053115 (2010)
120. X. Li, Q. Xue, X. Chang, L. Zhu, H. Zheng, J. Co_2 Util. **21**, 429–435 (2017)
121. X. Li, Y. Jin, Q. Xue, L. Zhu, W. Xing, H. Zheng, Z. Liu, J. Co_2 Util. **18**, 275–282 (2017)
122. K. Yao, M. Manjare, C.A. Barrett, B. Yang, T.T. Salguero, Y. Zhao, J. Phys. Chem. Lett. **3**, 2204–2208 (2012)
123. X. Shi, Y. Cheng, N.M. Pugno, H. Gao, Small **6**, 739–744 (2010)
124. Z. Liu, J. Gao, G. Zhang, Y. Cheng, Y.W. Zhang, Nanotechnology **28**, 385704 (2017)
125. Y. Wang, Y. Zhang, in *IEEE 65th Electronic Components and Technology Conference* (2015), pp. 1234–1239
126. H. Tarabkova, Z. Zelinger, P. Janda, Phys. Chem. Chem. Phys. **20**, 5900–5908 (2018)